Nanofabrication (2022) 7, 154-164
https://doi.org/10.37819/nanofab.007.255

eurasia

REVIEW ARTICLE

Check for updates

Bio-based semi-interpenetrating networks with nanoscale morphology and interconnected microporous structure

Samy Madbouly[a]

[a]*Penn State Behrend, 213K Jack Burke Res Center Erie Pennsylvania 16563, United States. Email: sum1541@psu.edu*

ABSTRACT

Creating new bio-based sustainable polymeric materials with similar or better performance than the petroleum-based counterparts has recently received considerable attention. It will have a significant positive impact on the environment and the sustainable polymer industry. This review article shows a relatively new method based on simultaneous in-situ polymerization and compatibilization of bio-based plant oil and biodegradable thermoplastic polymer to prepare semi-interpenetrating polymer networks (SINs) with unusual nano-scale morphology and interconnected porous structure will be summarized. The SINs were synthesized via cationic polymerization of tung oil in a homogenous solution of poly(ε-caprolactone) as a biodegradable, semi-crystalline, and biocompatible thermoplastic polymer. The degrees of miscibility, nanostructure morphology, and crystallinity was found to be composition-dependent. This relatively new blending method created a two-phase nanoscale morphology as small as 100 nm for blends with PCL contents of 20 and 30 wt.%. For higher PCL contents (e.g., 50 wt.% PCL blend), a co-continuous, interconnected microscale two-phase morphology was detected. The microporous structure of the SINs was also changed as a function of composition. For example, the interconnectivity and pore size was considerably decreased with increasing PCL content. Furthermore, a considerable decrease in the crystallization kinetics of PCL was observed as the PCL content is higher than or equal to 30 wt.%. While on the other hand, the crystallization kinetics accelerated significantly for 50 wt.%. This novel, low-cost strategy for preparing bio-based SINs with nanoscale morphology and interconnected three-dimensional cluster structures and desired properties should be widely used for creating new polymer systems.

ARTICLE HISTORY

Received: 25-07-2022
Revised: 12-11-2022
Accepted: 12-12-2022

KEYWORDS

plant oils;
semi-interpenetrating polymer networks;
bio-based polymers;
DMA;
morphology;
nanoscale

1. Introduction

As finite petroleum resources become scarcer and more expensive, the world is shifting its focus to sustainable, environmentally friendly products made from biorenewable biomass resources (Murawski *et al.*, 2019, Madbouly, 2022, Lu *et al.*, 2014, de Haro *et al.*, 2019, Arvin *et al.*, 2018, Chen *et al.*, 2019, Winnacker *et al.*, 2018, Björnerbäck, *et al.*, 2018, Ahmed *et al.*, 2019). Recently, considerable attention has been paid to developing new engineering materials based on biorenewable resources (Han *et al.*, 2023, Yang *et al.*, 2022, Mishra *et al.*, 2022, Zhang *et al.*,

2022, Sher *et al.*, 2022, Baghban *et al.*, 2021, Fan *et al.*, 2022, Kumar *et al.* 2022, Wu *et al.*, 2022). Vegetable oils are considered one of the world's cheapest and most abundant biorenewable resources (Gómez *et al*., 2022, Biswas *et al.*, 2022, Thomas *et al.*, 2022, Yan *et al.*, 2021, Gandini *et al.*, 2021, Kempanichkul *et al*, 2022). In addition to being available in large quantities, they are widely used for synthesising bio-based polymers with various advantages, such as low toxicity and inherent biodegradability. A triglyceride vegetable oil is composed mainly of saturated and unsaturated fatty acids that serve as the platform chemicals for polymer synthesis. Tung oil contains about 84% α-elaeostearic acid (cis-9, trans-11, trans-13-octadecatrienoic acid) triglyceride and can be readily obtained from the seeds of the tung tree in large quantities (Liu *et al.*, 2021). The large numbers of conjugated C=C bonds in the tung oil provide a very rapid polymerization process at room temperature. Therefore, tung oil can be found in many industrial applications, such as varnishes, paints, and many other related materials. In addition, tung oil can be polymerized into bio-based thermoset polymers via different polymerization techniques, such as cationic, free radical, and thermal polymerizations process (Omonov *et al*., 2022, Biswas *et al*., 2022, Pfister *et al* 2008). Brittle, dark brown tung oil-based thermoset can be obtained via cationically polymerized using boron trifluoride diethyl etherate (BFE) as initiator. Thermal and free radical copolymerization of tung oil with styrene and divinylbenzene have been used previously to improve the mechanical properties and reduce the brittleness issue of tung oil thermosets (Xia *et al.,* 2010). In this work, a variety of properties ranging from rigid plastics to tough and rubbery materials were synthesized based on this copolymerization process. The goal of this review article is to focus on the novel SINs of tung oil and poly(ε-caprolactone) (PCL) as both materials are biopolymers (PCL is petroleum-based semicrystalline thermoplastics but it is biodegradable as explained in more details in the next section).

The PCL is considered a bio-based thermoplastic, although it is originally from petroleum-based origin due to its biodegradability behavior. In addition, PCL is also biocompatible semicrystalline polyester with a glass-transition temperature (T_g) of about −60 °C and a melting temperature (T_m) of approximately 60°C (Tokiwa *et al.*, 2009, Madbouly *et al.*, 2003). The PCL has been used widely in many biomedical applications, such as sutures, adhesion barriers, scaffolds for tissue engineering, and long-term implants, due to its biocompatibility and biodegradability. The biodegradability behavior of PCL is related to hydrolysis in the physiological media of its ester linkages (Kim *et al*., 2008, Han *et al.*, 2009). PCL was also blended with numerous thermoplastic materials, including poly(styrene-co-acrylonitrile) (SAN), tetramethyl polycarbonate (TMPC), poly(lactic acid) (PLA), poly(methyl methacrylate) (PMMA), polycarbonate (PC), and poly(vinyl chloride) (PVC) (Madbouly *et al.*, 2004, Madbouly *et al*., 2007, Madbouly *et al.*, 2006, Takayama *et al.*, 2006, Abdelrazek *et al.*, 2016, Hirotsu *et al.*, 2000).

Blending is a common easy way to mix two or more polymers to produce new materials with diverse, tailored properties compared to individual polymer components. Due to the low entropy of mixing, most the polymer blends are immiscible and, in many cases, require a block or graft copolymer as a compatibilizer to improve the interfacial interaction and reduce the particle size. Immiscible polymer blends with macro-phase separation and large particle sizes have poor mechanical properties and limited industrial applications. Therefore, block/graft copolymer compatibilizers are crucial to improve the compatibility and thermodynamic stability of immiscible polymer blends. But most of these compatibilizers (block, graft or star copolymers) are expensive and commercially unavailable (Li *et al*., 2000; Madbouly *et al.*, 2006). A critical advantage of the polymerization and compatibilization method of blending is that no compatibilizer is needed, and compatible blends with excellent mechanical properties and nanoscale morphology can be easily achieved in this process which is not possible through other traditional blending methods, such as solvent cast or melt mixing.

This review article will summarise the cationic polymerization and compatibilization of tung oil and PCL in chloroform at room temperature to synthesize SINs with unique morphology and nanoscale structure. The thermomechanical properties will be evaluated as a temperature and blend composition function. In addition, the nanoscale morphology and the interconnected

porous structure will be investigated using SEM. The crystallization kinetics of the PCL in the blends will be studied using DSC measurements.

2. Synthesis of semi-interpenetrating tung oil/ PCL networks

The cationic polymerization of tung oil at room temperature is very aggressive. It produces brittle, dark material with very poor mechanical properties regardless of the concentration of the initiator (less than 0.1 wt.% of BFE). This speedy polymerization process of tung oil must be controlled and significantly inhibited via reducing the reactivity of BFE by dilution in chloroform. Chloroform is also an excellent common solvent for tung oil and PCL at room temperature. For all blend compositions, BFE was kept at a constant concentration of 2 wt.% relative to tung oil. Upon mixing tung oil with PCL and BFE in chloroform (25 wt.% solid content), the cationic polymerization of tung oil started immediately, and a yellow elastic gel was formed. After obtaining the gels, they were allowed to dry for approximately three days under vacuum at room temperature, followed by another two days at 60 °C. Fig. 1 shows the cationic polymerization of tung oil using BFE as a catalyst. The figure also demonstrates the FTIR for tung oil before and after cationic polymerization. The C═C bonds observed at 3013 cm^{-1} peak in the FTIR spectrum for pure tung oil (unreacted) disappeared after the cationic polymerization process (see Fig. 1), indicating a fully cured tung oil. The PCL reacted physically with tung oil during the cationic polymerization to form semi-interpenetrating polymer networks as described in the schematic diagram of Fig. 2. The entangled PCL polymer chains (blue) mixed with cross-linked tung oil (green) to form semi-interpenetrating polymer networks. After the drying process, the SINs of tung oil/PCL of different concentrations were investigated using DMA measurements.

Fig. 2 shows the temperature dependence of storage modulus (E') and loss tangent (tan δ) for fully cured and dried tung oil/PCL SINs of different compositions. The glass relaxation process (a-relaxation) obtained from the tan d peak maximum temperature for pure tung oil thermoset was observed at approximately 33 °C. For pure PCL, the a-relaxation process is extensive with low intensity compared to the pure tung oil thermoset and observed at about −38 °C. The α-relaxation process is a cooperative reorientation of the polymer chains and is

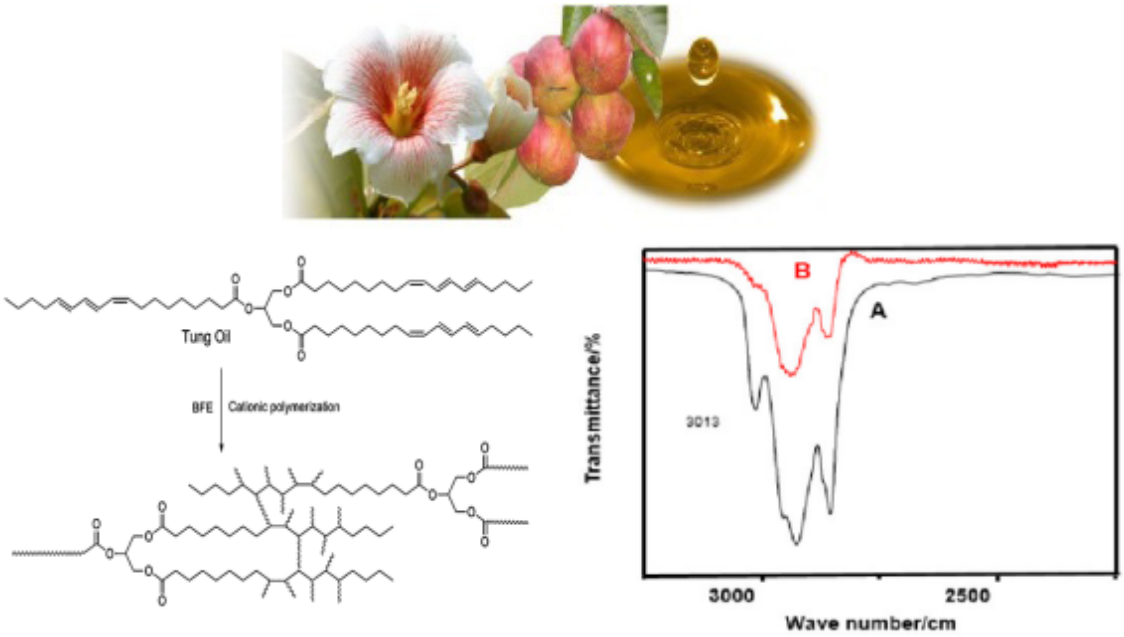

Figure 1. Picture for tung seeds and tung oil. Cationic polymerization and FTIR of tung oil before **(A)** and after **(B)** polymerization process. Adapted with permission from Madbouly et al., 2020. Photograph courtesy of The Wood Works Book Tool Co. Free domain: https://www.tungoil.com.au/.

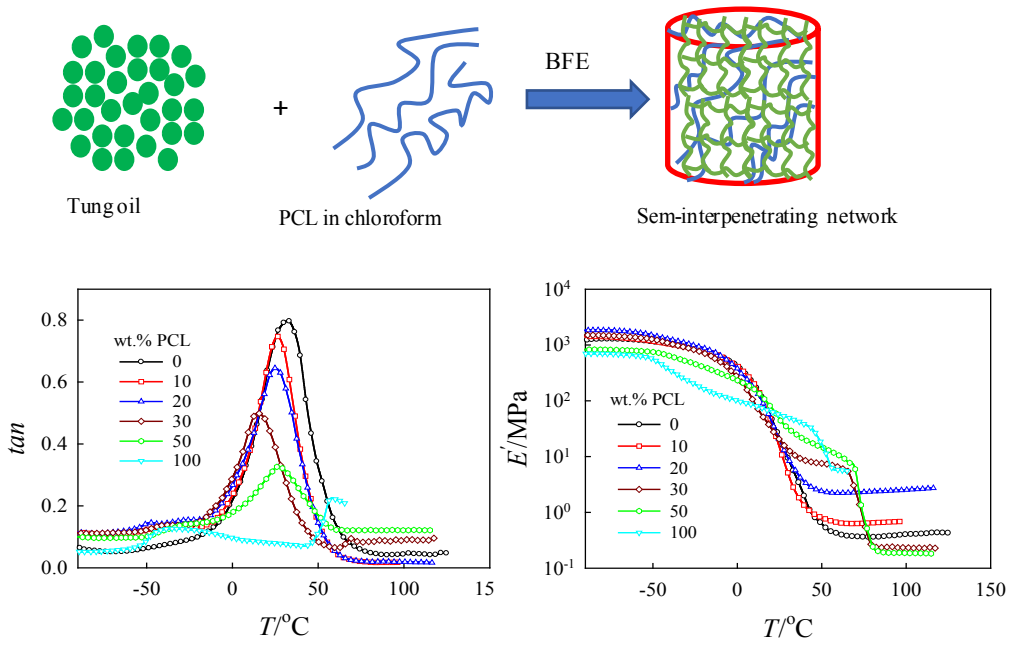

Figure 2. Schematic diagram for the formation of a Sem-interpenetrating network. Temperature dependence of E' and tan d for tung oil/PCL sem-interpenetrating network of different blend concentrations. It was adapted with permission from Madbouly *et al.*, 2014.

connected to the glass transition temperature T_g of the respective polymer component. From the analysis of the DMA data of tung oil and PCL blends, we can evaluate the miscibility in this semi-interpenetrating network. As seen in Fig. 2, the a-relaxation process of the tung oil strongly influence by blending with PCL. Tan *d* shifted to a lower temperature by increasing the PCL component content in the blend up to 30 wt.%. Based on this observation, it is suggested that the tung oil and PCL are completely miscible or partially miscible in this composition range. For 50 wt.% PCL blend, the a-relaxation process was shifted slightly to a lower temperature (only 5 °C for 50 wt.% while it was 20 °C for the tung oil/PCL 70/30 blend). This experimental finding indicated that the miscibility of PCL and tung oil decreases with increasing concentration of PCL above 30 wt.%.

3. Nanomorphology and interconnected cluster porous structures of semi-interpenetrating tung oil/PCL networks

Due to the low resolution and broadness of the a-relaxation peak of PCL, it is not accurate to rely on the DMA for evaluating the miscibility of tung oil thermoset and PCL thermoplastic blends. Therefore, a more reliable evaluation can be obtained from the morphology of the mixtures using a scanning electron microscope (SEM). Fig. 3 depicts the SEM morphology of SINs of oil/PCL of different compositions. The SEM photographs were used to evaluate and understand the miscibility of tung oil and PCL synthesized by this relatively new polymerization and compatibilization technique. The fully cured and dried SINs were fractured in liquid nitrogen and sputtered with thin layers of gold and then examined using a field emission scanning electron microscope (FE-SEM, FEI Quanta 250) operating at 10 kV under high vacuum. No morphology was observed for the tung oil/PCL 90/10 blend due to the formation of a one-phase structure or an utterly miscible blend. While on the other hand, the nanoscale structure of two-phase morphology with an average particle size as small as 100 nm was observed for blends with 20 ≤wt.% PCL≤ 40 as clearly seen in Fig. 3 (46). The white dispersed particles are the PCL phase, and the dark matrix is the tung oil phase.

Interconnected, the co-continuous microstructure was observed for the tun oil/PCL 50/50 blend, as seen in Fig. 3. According to the obtained morphologies, it is apparent that the in-situ

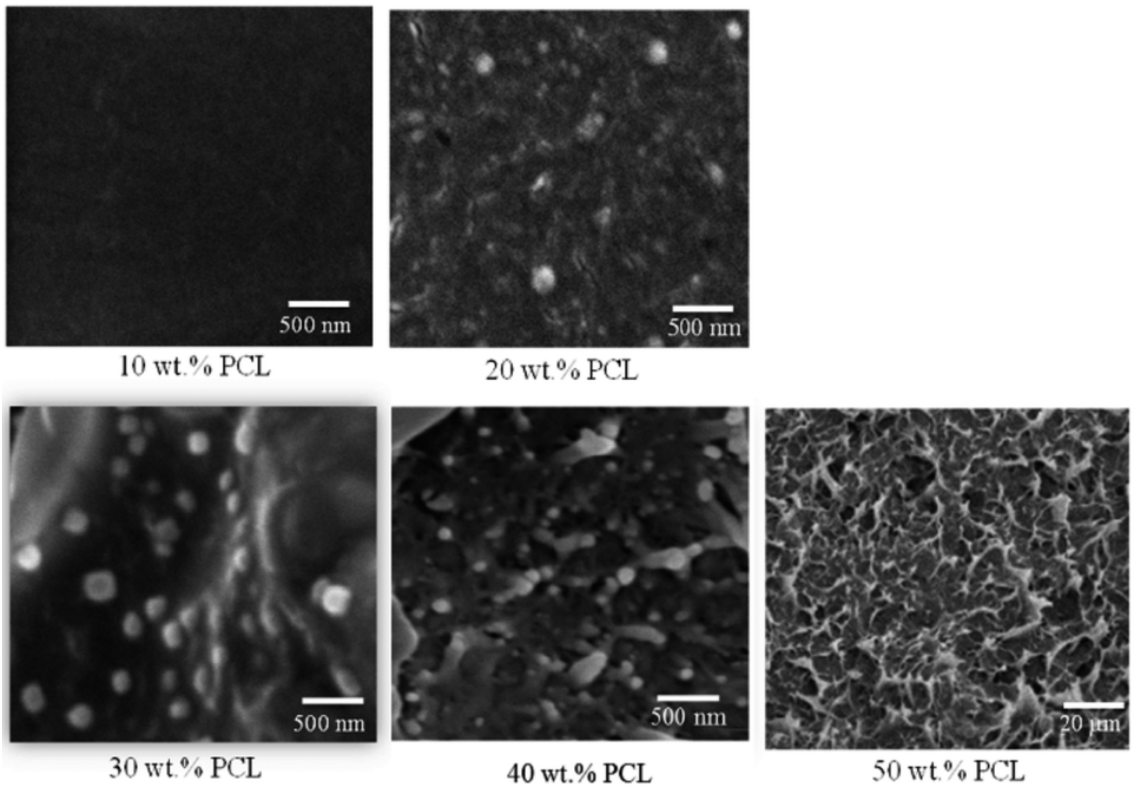

Figure 3. SEM morphologies for tung oil/PCL SINs of different concentrations. It is reproduced with permission from Madbouly *et al*., 2014.

polymerization and compatibilization of tung oil and PCL created unique different phase behaviors, including nano/microscales morphologies and completely miscible blends based on the different concentrations of the two components. This unique morphology and miscibility in the tung oil/PCL blends cannot be achieved in the standard blending methods, such as melt and solvent casting methods. In addition, the tung oil thermoset provides substantial morphology stability and eliminates particle-particle diffusion or coalescence at high temperatures. Based on the above, one can suggest that the simple strategy of the in-situ polymerization and compatibilization reviewed in this article can be considered a novel technique capable of creating new functional polymer blends or alloys that might be suitable for different industrial applications, such as shape-memory polymers, drug delivery, and tissue engineering.

Porous morphologies have been observed for tung oil/PCL blends with PCL concentrations lower than 50 wt.%, as clearly seen in Fig. 4 (45). The porous structure was observed for some blend concentrations due to the evaporation of the residual solvent during the drying process. The tendency of the blend to form a porous structure was dramatically decreased with increasing the PCL content in the blend. The thermoset tung oil created interconnected, clustered particles, while PCL dispersed as nanoparticles inside the cluster particle. The size of the interconnected, clustered particles for the blend with 30 wt.% PCL is much smaller than that of the blend with 20 wt.% PCL.

4. Crystallization kinetics of PCL in the semi-interpenetrating tung oil/PCL networks

It is well established that when semi-crystalline and amorphous polymers are blended, structural parameters, such as lamellar thickness, crystal interphase, and spherulitic growth rates are significantly influenced by the amorphous component, as in the current tung oil/PCL SINs (Alfonso *et al*., 1986, Braña *et al*., 1992, Vanneste *et al*., 1995). The melting point of the semi-crystalline polymer component is usually decreased by specific interaction with the amorphous component in the blend and by changes in the free energy required to form crystals.

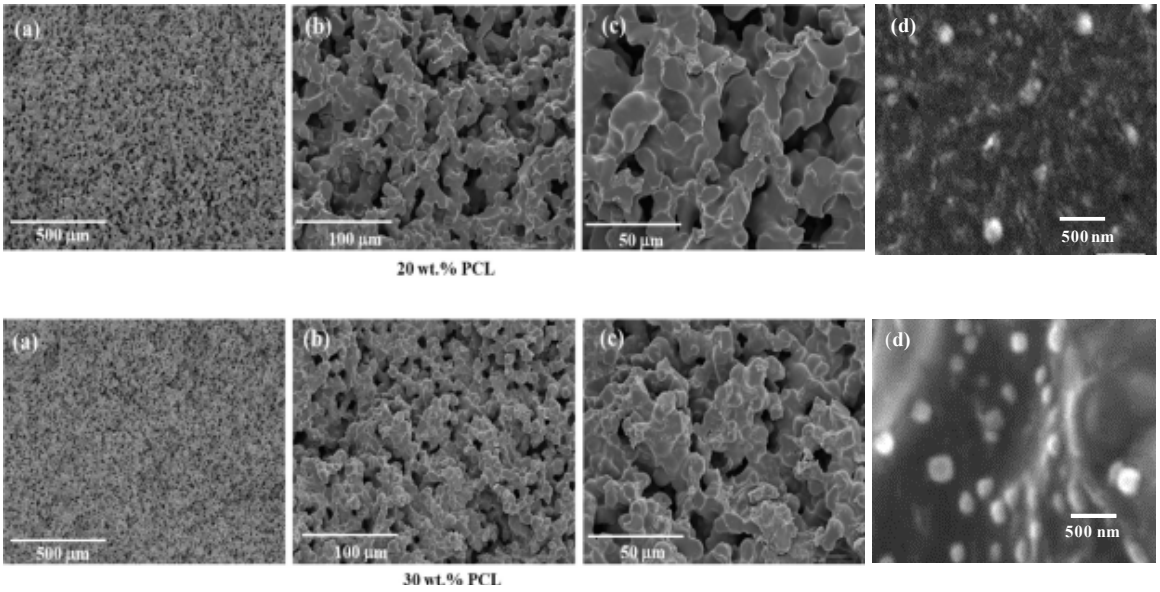

Figure 4. SEM photographs for fully cured porous and nanoscale structures for tung oil/PCL blends with 20 and 30 wt.% PCL at different magnifications **(a–d)**. It is adapted with permission from Madbouly *et al*., 2020.

For miscible polymer blends, a decrease in melting temperature and heat of fusion is commonly observed, and the decrease magnitude depends on the blend concentration. Fig. 5 depicts the DSC measurements for the PCL/tung oil SINs (second heating run) of different concentrations. In the blend, the melting temperature of PCL shifted to a lower temperature for the concentration range of 10 < PCL wt.% < 50, indicating miscibility or partial miscibility of the blends. No melting peak was observed for lower concentration range (e.g., 10 wt.% PCL) due to the complete miscibility of tung oil with 10 wt.% PCL in good agreement with the SEM morphology of Figure 3. The crystallization process of PCL in the interconnected, co-continuous structure of PCL/tung oil 50/50 blend greatly enhances, as seen in the shift of the melting point to a higher temperature. In addition, the blend (50/50) displayed bimodal peaks that might result from melt-recrystallization mechanisms. The melt-recrystallization occurs when crystals with defects or less perfect structures melt at lower temperatures and then reorganized into more perfect crystals that melt at higher temperatures.

The heat released during the crystallization process in the DSC is directly related to the macroscopic rate of the crystallization process. The isothermal crystallization process at different crystallization temperatures of pure PCL is demonstrated in

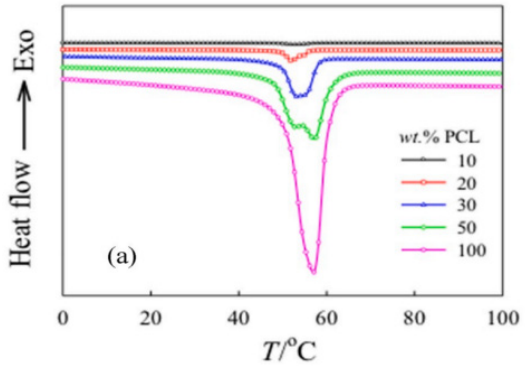

Figure 5. DSC thermograms (second heating run) for the melting temperature of tung oil/PCL SINs of different compositions. It is reproduced with permission from Madbouly *et al*., 2020.

Fig. 6a. For this isothermal crystallization process, all the samples were melted for 5 min at $T_m = 110$ °C and then the temperature decreased at a very high cooling rate (70 °C/min) to the crystallization temperature, T_c. The exothermic crystallization peak maximum shifted systematically to longer times with increasing the T_c. Based on the above, it is apparent that the higher the crystallization temperature is, the slower the isothermal crystallization process. Similar data was also evaluated for the PCL/tung oil 50/50 blend, as illustrated in Fig. 6b. As clearly seen in Fig. 6, the crystallization process of the PCL/tung oil 50/50 blend is significantly faster than that of pure PCL.

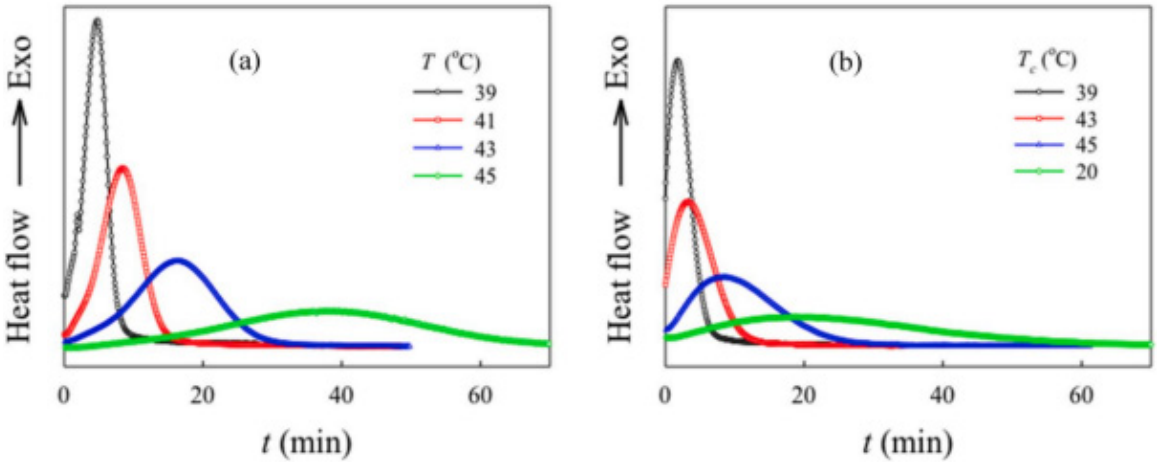

Figure 6. DSC thermograms for isothermal crystallization process, **(a)** pure PCL and **(b)** PCL/tung oil 50/50 blend at different crystallization temperatures T_c. Reproduced with permission from Madbouly *et al*., 2020.

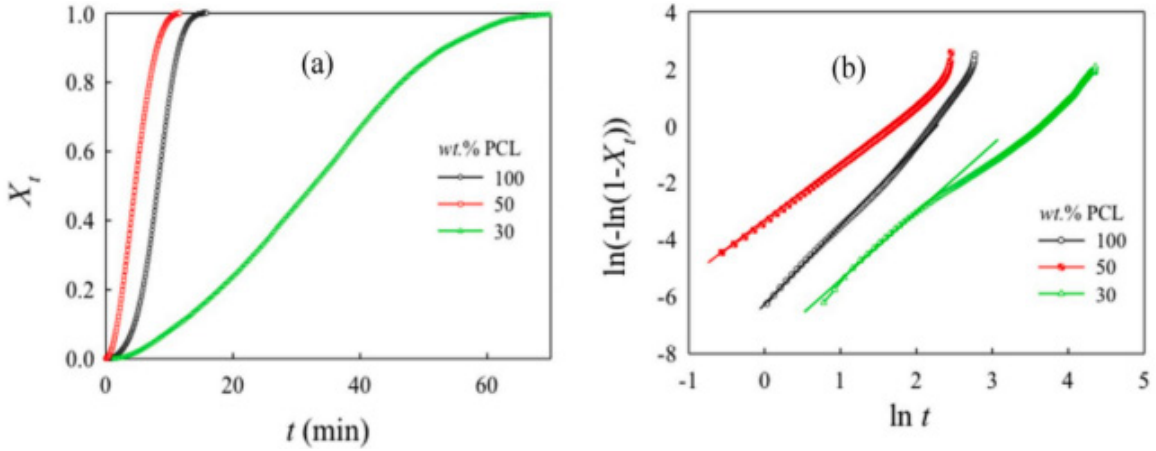

Figure 7. **(a)** Relative crystallinity (X_t) as a function of time for tung oil/PCL blends of different compositions at T_c = 41 °C; **(b)** Avrami plots for tung oil/PCL blends of different compositions at T_c = 41 °C. It is reproduced with permission from Madbouly *et al*., 2020.

For example, the peak maximum of the isothermal crystallization process of the pure PCL at T_c = 45 °C is approximately 40 min compared to 20 min for the 50/50 blend. The isothermal crystallization kinetics of PCL in the blends can be evaluated based on the Avrami equation (Gupta *et al.*, 2013, De Santis *et al.*, 2013):

$$X_t = 1 - \exp\left(e^{-kt^n}\right) \quad (1)$$

Where, X_t is the weight fraction of crystallization at a time t; and k is the crystallization rate constant, which depends on the crystallization temperature and includes the effects of nucleation and growth. At the same time, n is the Avrami exponent, which describes the crystal growth geometry and nucleation mechanism. The X_t can be evaluated from the exothermic DSC peaks of pure PCL and PCL/tung oil blends (see Fig. 6) according to the following equation:

$$X_t = \frac{\int_0^t \frac{dH}{dt} dt}{\int_0^\infty \frac{dH}{dt} dt} \quad (2)$$

Equation 2 describes the ratio of heat generated at time t and the total heat generated until the end of the crystallization process. The values of n and k (Avrami kinetic parameters) can be evaluated from the slope and intercept of the straight line of ln (-ln(1-X_t)) versus ln$t$. Figs. 7a and 7b demonstrate

PCL (wt. %)	T_c(°C)	n	log k
100	39	2.5	–1.86
	41	2.8	–2.78
	43	3.1	–4.0
	45	2.6	–4.6
50	39	2.4	–1.1
	41	2.1	–1.5
	43	1.9	–1.9
	45	2.4	–3.5
30	39	2.3	–2.4
	41	2.1	–3.2
	43	2.3	–5.1
	45	2.6	–6.3

Table 1. Avrami Kinetic parameters for isothermal crystallization kinetics of tung oil/PCL blends at different crystallization temperatures. It is reproduced with permission from Madbouly et al., 2020.

the X_t as a function of time and Avrami-type plots for tung oil/PCL blends of different compositions at T_c = 41 °C, respectively. Non-integral values of n are around 3 and were evaluated for all samples due to the athermal nucleation process followed by three-dimensional crystal growth (Kolmogorov 1937). The non-integral n cannot be used to predict the crystallization mechanism of PCL in the blends. The Avrami rate constant, k, decreased significantly with increasing crystallization temperature, as shown in Table 1. This data indicated that the crystallization rate decreased significantly with increasing T_c. Similar behavior has been observed in the blend with 30 wt.%PCL. However, on the other hand, the k value for PCL/tung oil 50/50 blend was about three times higher than that of pure PCL at a constant crystallization temperature. Based on the above result, one can conclude that the isothermal crystallization kinetics of PCL enhanced with the formation of co-continuous, interconnected morphology observed in the PCL/tung oil 50/50 blend.

5. Conclusion

Cationic polymerizing of tun oil in a homogeneous solution of PCL is a relatively new reactive blending method that can create polymer mixtures with different morphologies, miscibility, phase behavior, and crystallization rates without using traditional compatibilizers. One phase blend with no morphology was observed for blends with PCL contents ≤ 10 wt.%. For higher PCL concentrations < 50 wt.%, two-phase with nanoscale morphologies as small as 100 nm of PCL phase in tun oil matrix were detected. Highly interconnected, co-continuous two-phase morphology was observed for the tung oil/PCL 50/50 blend. These unique morphologies and miscibility in the tung oil/PCL blends cannot be achieved in the standard blending methods, such as melt and solvent casting methods. In addition, the tung oil thermoset provides substantial morphology stability and eliminates particle-particle diffusion or coalescence at high temperatures. Porous morphologies have been observed for tung oil/PCL blends with PCL concentrations lower than 50 wt.%. The porous structure was observed for some blend concentrations due to the evaporation of the residual solvent during the drying process. The tendency of the blend to form a porous structure was dramatically decreased with increasing the PCL content in the blend. The effect of tung oil thermoset on the isothermal crystallization kinetics was summarized for different blend concentrations. The blends' morphology and miscibility were found to impact the PCL crystallization process significantly. For miscible and partially miscible blends (blends with PCL contents ≥ 30 wt.%), the isothermal crystallization process retarded greatly. For blend with micro-interconnected, co-continuous two-phase morphology (50/50 wt.% blend), the isothermal crystallization kinetics of PCL was accelerated significantly. Finally, this relatively new and simple strategy for in-situ polymerization and compatibilization reviewed in this article can be considered a novel technique to create unique functional polymer blends or alloys that might be suitable for different applications, such as shape-memory polymers, drug delivery, and tissue engineering.

References

Abdelrazek, E. M., Hezma, A. M., El-Khodary, A., & Elzayat, A. M. (2016). Spectroscopic studies and thermal properties of PCL/PMMA biopolymer blend. *Egyptian Journal of basic and applied sciences*, *3*(1), 10-15.

Ahmed, S. T., Leferink, N. G., & Scrutton, N. S. (2019). Chemo-enzymatic routes towards the synthesis of bio-based monomers and polymers. *Molecular Catalysis*, *467*, 95-110.

Alfonso, G. C., & Russell, T. P. (1986). Kinetics of crystallization in semicrystalline/amorphous polymer mixtures. *Macromolecules*, *19*(4), 1143-1152.

Arvin, Z. Y., Rahimi, A., & Webster, D. C. (2018). High performance bio-based thermosets from dimethacrylated epoxidized sucrose soyate (DMESS). *European Polymer Journal*, *99*, 202-211.

Baghban, S. A., Ebrahimi, M., Khorasani, M., & Bagheri-Khoulenjani, S. (2021). Design of different self-stratifying patterns in a VOC-free light-curable coating containing bio-renewable materials: Study on formulation and processing conditions. *Progress in Organic Coatings*, *161*, 106519.

Biswas, E., Silva, J. A. C., Khan, M., & Quirino, R. L. (2022). Synthesis and Properties of Bio-Based Composites from Vegetable Oils and Starch. *Coatings*, *12*(8), 1119.

Björnerbäck, F., & Hedin, N. (2018). Microporous humins prepared from sugars and bio-based polymers in concentrated sulfuric acid. *ACS Sustainable Chemistry & Engineering*, *7*(1), 1018-1027.

Braña, M. C., & Gedde, U. W. (1992). Morphology of binary blends of linear and branched polyethylene: composition and crystallization-temperature dependence. *Polymer*, *33*(15), 3123-3136.

Chen, N., Lin, Q., Zheng, P., Rao, J., Zeng, Q., & Sun, J. (2019). A sustainable bio-based adhesive derived from defatted soy flour and epichlorohydrin. *Wood Science and Technology*, *53*(4), 801-817.

De Haro, J. C., Allegretti, C., Smit, A. T., Turri, S., D'Arrigo, P., & Griffini, G. (2019). Biobased polyurethane coatings with high biomass content: tailored properties by lignin selection. *ACS Sustainable Chemistry & Engineering*, *7*(13), 11700-11711.

De Santis, F., & Pantani, R. (2013). Nucleation density and growth rate of polypropylene measured by calorimetric experiments. *Journal of thermal analysis and calorimetry*, *112*(3), 1481-1488.

Fan, J., Abedi-Dorcheh, K., Sadat Vaziri, A., Kazemi-Aghdam, F., Rafieyan, S., Sohrabinejad, M., ... & Jahed, V. (2022). A Review of Recent Advances in Natural Polymer-Based Scaffolds for Musculoskeletal Tissue Engineering. *Polymers*, *14*(10), 2097.

Gandini, A., & M. Lacerda, T. (2021). Monomers and Macromolecular Materials from Renewable Resources: State of the Art and Perspectives. *Molecules*, *27*(1), 159.

Gómez, C., Inciarte, H., Orozco, L. M., Cardona, S., Villada, Y., & Rios, L. (2022). Interesterification and blending with Sacha Inchi oil as strategies to improve the drying properties of Castor Oil. *Progress in Organic Coatings*, *162*, 106572.

Gupta, A., & Choudhary, V. (2013). Isothermal crystallization kinetics of poly (trimethylene terephthalate)/multiwall carbon nanotubes composites. *Journal of thermal analysis and calorimetry*, *114*(2), 643-651.

Han, J., Chen, T. X., Branford-White, C. J., & Zhu, L. M. (2009). Electrospun shikonin-loaded PCL/PTMC composite fiber mats with potential biomedical applications. *International journal of pharmaceutics*, *382*(1-2), 215-221.

Han, X., Chen, L., Yanilmaz, M., Lu, X., Yang, K., Hu, K., ... & Zhang, X. (2023). From Nature, Requite to Nature: Bio-based Cellulose and Its Derivatives for Construction of Green Zinc Batteries. *Chemical Engineering Journal*, *454*(3), 140311.

Hirotsu, T., Ketelaars, A. A. J., & Nakayama, K. (2000). Biodegradation of poly (ε-caprolactone)–polycarbonate blend sheets. *Polymer Degradation and Stability*, *68*(3), 311-316.

Kempanichkul, A., Piroonpan, T., Kongkaoropham, P., Wongkrongsak, S., Katemake, P., & Pasanphan, W. (2022). Electron beam-cured linseed oil-Diacrylate blends as a green alternative to overprint varnishes: Monitoring curing efficiency and surface coating properties. *Radiation Physics and Chemistry*, *199*, 110350.

Kim, H., Choi, S. H., Ryu, J. J., Koh, S. Y., Park, J. H., & Lee, I. S. (2008). The biocompatibility of SLA-treated titanium implants. *Biomedical Materials*, *3*(2), 025011.

Kolmogorov, A. N. (1937). On the statistical theory of the crystallization of metals. *Bull. Acad. Sci. USSR, Math. Ser.* 1(3):355-359.

Kumar, S., Abdellah, M. H., Alammar, A., & Szekely, G. (2022). Biorenewable Nanocomposite Materials in Membrane Separations. In *Biorenewable Nanocomposite Materials, Vol. 2: Desalination and Wastewater Remediation* (pp. 189-235). American Chemical Society.

Li, F., & Larock, R. C. (2000). Thermosetting polymers from cationic copolymerization

of tung oil: Synthesis and characterization. *Journal of Applied Polymer Science*, *78*(5), 1044-1056.

Liu, M., Lyu, S., Peng, L., Lyu, J., & Huang, Z. (2021). Radiata pine fretboard material of string instruments treated with furfuryl alcohol followed by tung oil. *Holzforschung*, *75*(5), 480-493.

Lu, H., Madbouly, S. A., Schrader, J. A., Kessler, M. R., Grewell, D., & Graves, W. R. (2014). Novel bio-based composites of polyhydroxyalkanoate (PHA)/distillers dried grains with solubles (DDGS). *RSC advances*, *4*(75), 39802-39808.

Madbouly, S. A., & Ougizawa, T. (2003). Rheological investigation of shear-induced crystallization of poly (ε-caprolactone). *Journal of Macromolecular Science, Part B*, *42*(2), 269-281.

Madbouly, S. A., & Ougizawa, T. (2004). Isothermal Crystallization of Poly (ε-caprolactone) in Blend with Poly (styrene-co-acrylonitrile): Influence of Phase Separation Process. *Macromolecular Chemistry and Physics*, *205*(14), 1923-1931.

Madbouly, S. A., Abdou, N. Y., & Mansour, A. A. (2006). Isothermal crystallization kinetics of poly (ε-caprolactone) with tetramethyl polycarbonate and poly (styrene-co-acrylonitrile) blends using broadband dielectric spectroscopy. *Macromolecular Chemistry and Physics*, *207*(11), 978-986.

Madbouly, S. A., Otaigbe, J. U., & Ougizawa, T. (2006). Morphology and properties of novel blends prepared from simultaneous in situ polymerization and compatibilization of macrocyclic carbonates and maleated poly (propylene). *Macromolecular Chemistry and Physics*, *207*(14), 1233-1243.

Madbouly, S. A. (2007). Isothermal crystallization kinetics in binary miscible blend of poly (ε-caprolactone)/tetramethyl polycarbonate. *Journal of applied polymer science*, *103*(5), 3307-3315.

Madbouly, S. A., Liu, K., Xia, Y., & Kessler, M. R. (2014). Semi-interpenetrating polymer networks prepared from in situ cationic polymerization of bio-based tung oil with biodegradable polycaprolactone. *RSC Advances*, *4*(13), 6710-6718.

Madbouly, S. A. (2020). Nano/micro-scale morphologies of semi-interpenetrating poly (ε-caprolactone)/tung oil polymer networks: Isothermal and non-isothermal crystallization kinetics. *Polymer Testing*, *89*, 106586.

Madbouly, S. A., & Kessler, M. R. (2020). Preparation of nanoscale semi-IPNs with an interconnected microporous structure via cationic polymerization of bio-based tung oil in a homogeneous solution of poly (ε-caprolactone). *ACS omega*, *5*(17), 9977-9984.

Madbouly, S. A. (2022). Bio-based castor oil and lignin sulphonate: aqueous dispersions and shape-memory films. *Biomaterials and Polymers Horizon*, *1*(2).

Mishra, K., Devi, N., Siwal, S. S., Zhang, Q., Alsanie, W. F., Scarpa, F., & Thakur, V. K. (2022). Ionic Liquid-Based Polymer Nanocomposites for Sensors, Energy, Biomedicine, and Environmental Applications: Roadmap to the Future. *Advanced Science*, *9*(26), 2202187.

Murawski, A., Diaz, R., Inglesby, S., Delabar, K., & Quirino, R. L. (2019). Synthesis of bio-based polymer composites: fabrication, fillers, properties, and challenges. In *Polymer nanocomposites in biomedical engineering* (pp. 29-55). Springer, Cham.

Omonov, T. S., Patel, V. R., & Curtis, J. M. (2022). Biobased Thermosets from Epoxidized Linseed Oil and Its Methyl Esters. *ACS Applied Polymer Materials*, *4*(9), 6531-6542.

Pfister, D. P., Baker, J. R., Henna, P. H., Lu, Y., & Larock, R. C. (2008). Preparation and properties of tung oil-based composites using spent germ as a natural filler. *Journal of applied polymer science*, *108*(6), 3618-3625.

Sher, F., Ilyas, M., Ilyas, M., Liaqat, U., Lima, E. C., Sillanpää, M., & Klemeš, J. J. (2022). Biorenewable Nanocomposites as Robust Materials for Energy Storage Applications. In *Biorenewable Nanocomposite Materials, Vol. 1: Electrocatalysts and Energy Storage* (pp. 197-224). American Chemical Society.

Takayama, T., & Todo, M. (2006). Improvement of impact fracture properties of PLA/PCL polymer blend due to LTI addition. *Journal of materials science*, *41*(15), 4989-4992.

Thomas, J., & Soucek, M. D. (2022). Cationic Copolymers of Norbornylized Seed Oils for Fiber-Reinforced Composite Applications. *ACS omega*, *7*(38), 33949-33962.

Tokiwa, Y., Calabia, B. P., Ugwu, C. U., & Aiba, S. (2009). Biodegradability of plastics. *International journal of molecular sciences*, *10*(9), 3722-3742.

Vanneste, M., & Groeninckx, G. (1995). Ternary blends of PCL, SAN15 and SMA14: miscibility, crystallization and melting behaviour, and semicrystalline morphology. *Polymer*, *36*(22), 4253-4261.

Winnacker, M. (2018). Pinenes: Abundant and renewable building blocks for a variety of sustainable polymers. *Angewandte Chemie International Edition*, *57*(44), 14362-14371.

Wu, S., Shi, W., Li, K., Cai, J., & Chen, L. (2022). Recent advances on sustainable bio-based materials for water treatment: fabrication, modification and application. *Journal of Environmental Chemical Engineering*, *10*(6), 108921.

Xia, Y., & Larock, R. C. (2010). Castor oil-based thermosets with varied crosslink densities prepared by ring-opening metathesis polymerization (ROMP). *Polymer*, *51*(12), 2508-2514.

Yang, W., Ding, H., Puglia, D., Kenny, J. M., Liu, T., Guo, J., ... & Lemstra, P. J. (2022). Bio-renewable polymers based on lignin-derived phenol monomers: Synthesis, applications, and perspectives. *SusMat*.

Yan, Y., Wu, J., Wang, Y., Fang, X., Wang, Z., Yang, G., & Hua, Z. (2021). Strong and UV-Responsive Plant Oil-Based Ethanol Aqueous Adhesives Fabricated Via Surfactant-free RAFT-Mediated Emulsion Polymerization. *ACS Sustainable Chemistry & Engineering*, *9*(40), 13695-13702.

Zhang, C., Xue, J., Yang, X., Ke, Y., Ou, R., Wang, Y., & Wang, Q. (2022). From plant phenols to novel bio-based polymers. *Progress in Polymer Science*, *125*, 101473.